ELSEVIER

Chemical Engineering Journal 141 (2008) 169–179

Chemical Engineering Journal

www.elsevier.com/locate/cej

Characterization of fluidization behavior in the bottom region of CFB risers

Haiyan Zhu, Jesse Zhu *

Department of Chemical and Biochemical Engineering, University of Western Ontario, 1151 Richmond Street, London, Ontario, Canada N6A 5B9

Received 22 January 2007; received in revised form 11 December 2007; accepted 13 December 2007

Abstract

The hydrodynamic characteristics in the bottom region of circulating fluidized bed (CFB) risers with fluid catalytic cracking (FCC) particles were studied over a wide range of operating conditions. The results included radial solids concentration and corresponding radial profiles of standard deviation, particle velocity profiles, and probability density distributions. Comparisons were made between the flow structures in the riser bottom region and those in bubbling and turbulent fluidized beds.

Keywords: Circulating fluidized bed; Fluidization regime; Solids concentration; Particle velocity

1. Introduction

Since 1970s, circulating fluidized beds (CFBs) have been widely applied in the chemical, petrochemical, metallurgical, environmental and energy industries [1–3]. In order to continuously improve the design efficiency and performance of the existing industrial processes and facilitate new applications, intensive studies have been conducted to obtain more detailed and reliable fundamental knowledge about CFB [4–7]. Although the hydrodynamics of CFBs have been investigated to some extent both in industry and in academia, much remains to be known about this special multi-phase fluidization system, especially in its bottom dense region [1].

It is well known that, the solids holdup in a CFB riser varies strongly with axial and radial positions. This non-uniform solids distribution can affect the flow structures and further affect the reaction rates, the mass and heat transfer, and erosion within the riser [8]. Due to its importance, the solids distribution in a riser has been the subject of a number of studies reported in the literature. Previous studies have shown that, in general, the axial profiles of solids concentration in a CFB riser can be divided into three regions: a dense region at the bottom, a dilute region at the top, and a transition region between, as shown in Fig. 1 [4,5,9–11]. The operating conditions [5,11,12], system structure [13,14], solids inventory [15], particle and gas properties [16,17] have all been found to influence the solids distributions in the riser. For example, at a constant gas velocity, increasing solids flow rate leads to a denser bottom region and an increased dense region height, whereas an increase in gas velocity at a constant solids flow rate reduces the height of the dense region and causes dilution of this region [18].

Research on the local flow structures in CFB risers reveals that the radial solids distribution profiles are influenced by both the operating conditions and height. It is generally accepted that, in the upper dilute region of a riser, there exists a core–annulus flow structure with a rapid upflowing dilute core region surrounded by a relatively dense annulus, where solids may travel downwards on average or upwards at a much slower velocity [5,16,19–21]. Decreasing the superficial gas velocity or increasing the solids circulation rate has been found to steepen the radial voidage profile, and the extent of lateral solids segregation increases with increasing solids mass flux [22].

In contrast to the upper dilute region, which has received more attention and whose flow structure is relatively clear now, there is significant controversy in the literature on the actual mechanics in the bottom region and what flow regimes can be applied to this region. There are mainly two opinions in the literature:

(1) *Bubbling flow regime.* Svensson et al. [23] suggested from pressure measurements that the bottom region of

Abbreviations: CFB, circulating fluidized bed; BFB, bubbling fluidized bed; TFB, turbulent fluidized bed.

* Corresponding author. Tel.: +1 519 661 3807; fax: +1 519 850 2441.
E-mail address: jzhu@uwo.ca (J. Zhu).

1385-8947/$ – see front matter © 2008 Elsevier B.V. All rights reserved.
doi:10.1016/j.cej.2007.12.015

Nomenclature

G_s	solids flow rate (kg/(m^2 s))
r	radial coordinate (m)
R	radius of column (m)
U_g	superficial velocity of gas (m/s)
$V_{p,up}$	mean upflowing particle velocity
$V_{p,down}$	mean downflowing particle velocity
Z	height above gas distributor (m)

Greek symbols

ε_s	solids volume concentration
$\bar{\varepsilon}_s$	solids average volume concentration
σ	standard deviation

CFB risers was in an 'exploding bubble regime'. With a momentum probe and capacitance tomography technique Rhodes et al. [5] found that a bubbling flow regime with a core–annulus flow structure existed in the lower dense region. Both the two studies used Group B particles. In the study of Svensson et al. [23], the particle diameter was 320 μm with 2600 kg/m^3 density and in the study of Rhodes et al. [5], the particle diameter was 100 μm with 2650 kg/m^3 density.

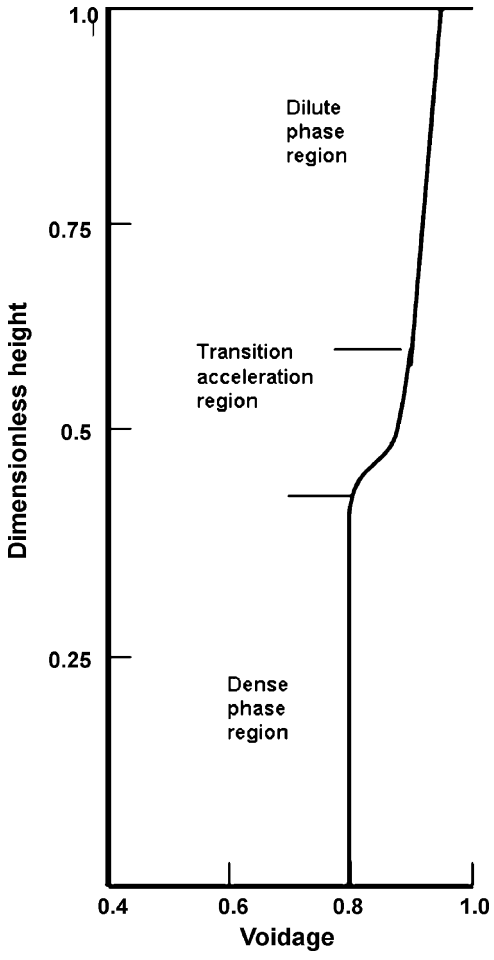

Fig. 1. Axial bed voidage profile observed in the riser of circulating fluidized bed [1].

(2) *Turbulent flow regime.* With the measurements of differential pressure probe and solids momentum probe using FCC particles (d_p = 51.9 μm and ρ_p = 2650 kg/m^3), Bai et al. [24] described the bottom dense region as "a more radial homogeneous cluster-dominating turbulent pattern".

The above investigations show that, although previous studies have given some insight into the flow structure of the bottom region in CFB risers, up to now no general agreement about the flow structure in this region has been reached and this area of fluidization research has not received much attention so far. The flow structures in the bottom region are critical to the overall hydrodynamics in circulating fluidized beds. The bottom region serves as an initial gas–solid mixing section for the whole riser. Due to the high solids holdup and the high reactant concentrations, a significant portion of the reaction can take place in this region [25,26]. Moreover, good descriptions of the flow behavior are essential to develop and valid predictable reactor models. Most of the early efforts were in CFB research focused on the upper dilute region or under very low solids mass flux conditions [27–31]. This may partly be due to the relatively complex flow behavior under high-density conditions, especially in the bottom region. Therefore, it is necessary to study the hydrodynamics of gas–solid flow in the bottom region of risers under high-flux and/or high-density conditions.

The purpose of this study was to provide a new perspective and detailed picture of the flow state in the CFB riser bottom region based on the measurements of local solids concentration and velocity over a wide range of operating conditions. The present work also examined the influence of riser diameter.

2. Experimental system

Experiments were conducted in a circulating fluidized bed system shown schematically in Fig. 2. It consisted of two 10-m long risers of 0.076- and 0.203-m diameters. The same downcomer (storage tank) of internal diameter 0.32 m was utilized. Solids used were spent fluid catalytic cracking (FCC) catalyst particles having a Sauter mean diameter of 65 μm and a particle density of 1780 kg/m^3. After passing a short inclined pipe section, the solids from the storage tank entered the riser bottom 0.21 m above the gas distributor and were accelerated by air in near ambient temperature. At the riser top, the entrained solids passed through a smooth exit into the primary, secondary and tertiary cyclone. The final gas–solids separation took place in a large capacity bag filter from which collected particles were recycled to the downcomer. Air was introduced into the riser bottoms through perforated distributor plates of 14% free area.

Reflective-type optical fiber probes are effective tools for measuring local voidage in fluidized beds, and they have been widely used (e.g. [32–35]). Their small size does not significantly disturb the overall flow structure [36]. More importantly, they are nearly free of interference by temperature, humidity,

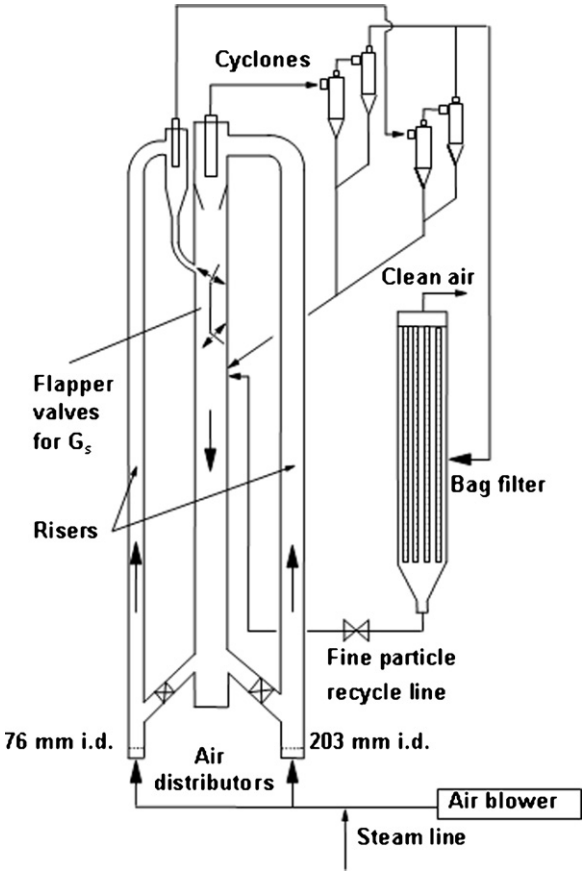

Fig. 2. Schematic drawing of the circulating fluidized bed risers.

electrostatics and electromagnetic fields [37]. This study utilized a model PV-5 optical fiber probe which was developed by the Institute of Process Engineering, Chinese Academy of Sciences, Beijing, China. The probe was capable of measuring instantaneous solids concentration and velocity simultaneously. The probe, 4 mm in diameter, consisted of two sub-probes, each with an active tip area of 1 mm × 1 mm cross-section. The separation distance between the two tips was 1.7 mm. Each sub-probe consisted of both light-emitting and light-receiving quartz fibers, arranged in alternating arrays of emitting and receiving layers of fibers. The diameter of each fiber was 25 μm. In order to prevent particles from occupying the probe's blind zone, a 0.2-mm thick glass cover was placed over the probe tip. A schematic drawing is shown in Fig. 3. The light reflected by the particles was transmitted by the fibers to two photo-multipliers, one for each probe where it was converted into voltage signals. The voltage signals were then acquired by a PC-based data sampling system.

Because of the non-linear relationship between the output signals of the optical fiber probe and the solids concentration in the measurement volume [37,38], reliable calibration was required to ensure accurate measurements. In this study, the calibration was carried out in a gas–solid downer system. The particles used in the calibration were the same to those used in the fluidization tests in this study. The calibrated solids volume concentration ranged from 0 to 0.56 corresponding to the solids concentration in a loosely packed bed. The downer column diameter was

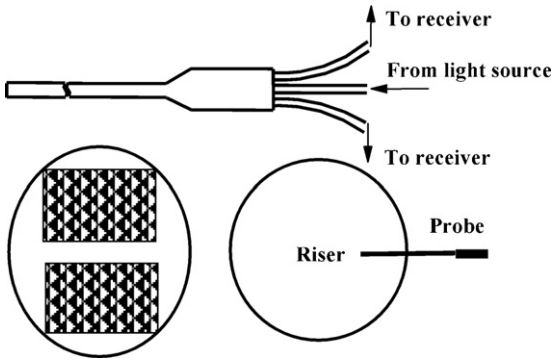

Fig. 3. Schematic of the solids concentration–velocity fiber optic probe.

13 mm, which was small enough to get a local measurement from cross-sectionally averaged value. Details of the calibration system were described by Zhang et al. [37]. The two sub-probes enable measurement of the instantaneous local solids velocity. Vertically moving particles, in principle, passed the tips of both sub-probes vertically aligned one above the other, and gave similar signals, but shifted in time. The time delay, obtained by cross-correlating the two signal series, yields the velocity of the particles moving in front of the probe tip. Fig. 3 shows the optical measurement system and details of the probe tips. With the aid of this measuring technique, it was possible to derive a virtually complete picture of local solids flows at the bottom of riser.

The probe was mounted at an axial level of 1.5 m above the gas distributor and was laterally movable. Local solids volume concentration (ε_s) and velocity (V_p) were measured at eleven radial positions ($r/R = 0.0$, 0.16, 0.38, 0.50, 0.59, 0.67, 0.74, 0.81, 0.87, 0.92 and 0.98) under a wide range of operating conditions given in Table 1. To ensure the validity and repeatability of sampled signals, the sampling time was 13.1 s with a frequency of 50 kHz and the measurements were repeated at least five times at each position. This combination of the sampling rate and duration ensured that the full spectra of hydrodynamic signals of interest were captured from the fluidized bed. For the calculation of the solids velocities, an integration time t of 20.5 ms was set, and there were 630 groups for each sampling. Valid particle velocity values must have a cross-correlation coefficient higher than 0.6 [39]. Time-averaged particle velocity was calculated over the sampling period of 13.1 s. The upward and downward particle movements were determined based on the maximum cross-correlation coefficient from the forward and backward correlation of the signals, respectively.

Table 1
Operating conditions in two risers

Riser i.d. (m)	U_g (m/s)	G_s (kg/(m^2 s))
0.076, 0.203	2.0	50
0.076, 0.203	3.5	50
0.076	8.0	50
0.076	8.0	200
0.076	8.0	400

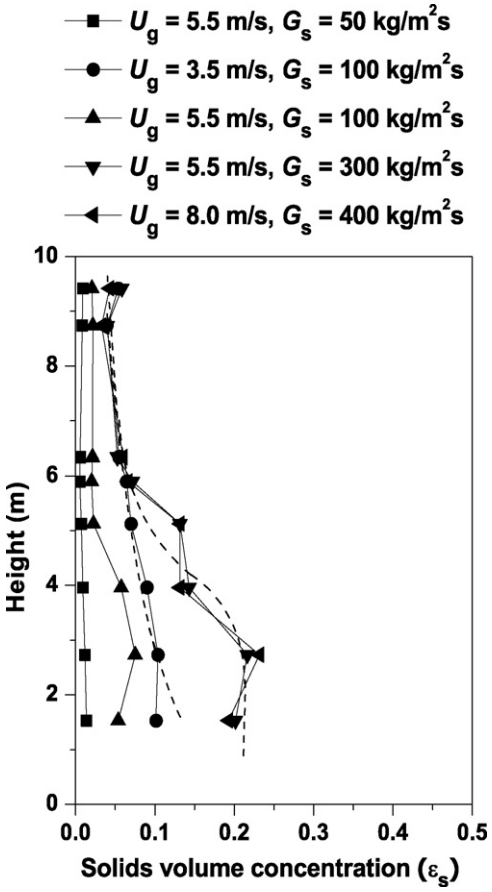

Fig. 4. Axial solids holdup distributions in the 0.076-m i.d. riser of our twin riser system [18,40].

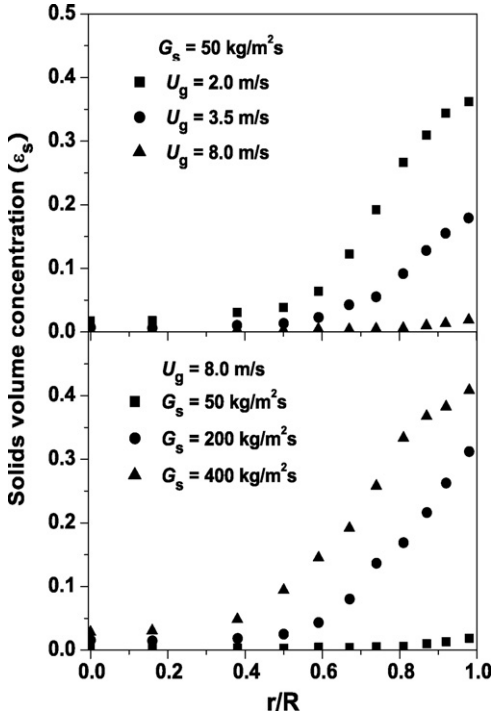

Fig. 5. Effects of operation conditions on radial solids concentration (Z = 1.5 m, 0.076-m i.d.).

3. Results and discussion

3.1. Density variation in the bottom region

Fig. 4 plots the axial profiles of mean solids concentrations in 76-mm i.d. riser for different solids flow rates (G_s = 50–400 kg/(m^2 s)), and superficial gas velocities (U_g = 3.5–8 m/s) obtained from our previous studies [18,40]. Measurements were taken in the riser, by averaging the local solids concentrations measured at 10 radial positions (excluding the center point). The axial solids distribution profiles clearly provide evidence that the solids concentration is a strong function of bed height and operating conditions. Depending on the operating conditions, three axial solids distribution profiles can be observed in Fig. 4: (1) dilute uniform axial profile with constant solids volume concentration ($\bar{\varepsilon}_s < 0.02$) throughout the entire riser; (2) exponential profile with continuous decreasing solids concentration with the bed height (if the bottom-most data point Z = 1.5 m was left out) until reaching a constant value at the upper section of the riser; and (3) S-shaped profile with a stable dense region at the bottom ($\bar{\varepsilon}_s > 0.1$) and dilute region at the top of the riser, suggesting limited variation in solids concentration. Similar axial solids concentration profiles have been reported elsewhere (e.g. [5,8,25,41–43]). According to cross-sectional averaged solids concentration ($\bar{\varepsilon}_s$), two kinds of riser bottom region can be defined: (1) dilute bottom region with $\bar{\varepsilon}_s < 0.1$, without the formation of the S-shaped axial solids concentration profile and (2) dense bottom region with $\bar{\varepsilon}_s > 0.1$, leading to a S-shaped axial solids concentration profile. This tentative demarcation of $\bar{\varepsilon}_s > 0.1$ was based on our current experimental data.

3.2. Radial solids distribution in the bottom region

Fig. 5 plots the effects of operating conditions (U_g, G_s) on the radial profiles of time-averaged solids concentration in the bottom region (Z = 1.5 m) of the 0.076-m i.d. riser. In general, the radial solids concentration profile is non-uniform under all operating conditions, and this non-uniformity increased with increasing solids circulation rate, G_s, and/or decreasing superficial gas velocity, U_g. The shape of the radial profiles appears to have two regions at high-density conditions: a central region up to r/R = 0.5–0.6, where the solids concentration is low and relatively constant, and a wall region of higher solids concentration where the increase in ε_s towards the wall augments significantly. Such core–annulus structure was also reported in other studies (e.g. [5,21,25,44]). It is worth noting that the solids volume concentrations in the core region of riser ($0 < r/R < 0.5$) is not significantly sensitive to the changes in operating conditions. At G_s = 50 kg/(m^2 s) and U_g = 8.0 m/s, the radial profile is nearly flat over the whole cross-section, with the overall cross-sectional solids concentration of 0.01, which is the characteristic of the dilute pneumatic transport regime.

The cross-sectional average solids concentrations for the above five operating conditions are summarized in Table 2. Combining the axial solids concentration profiles (Fig. 4) and the

Table 2
Cross-sectional average solids concentration

	$\bar{\varepsilon}_s$
$U_g = 2.0$ m/s, $G_s = 50$ kg/(m^2 s)	0.16
$U_g = 3.5$ m/s, $G_s = 50$ kg/(m^2 s)	0.08
$U_g = 8.0$ m/s, $G_s = 50$ kg/(m^2 s)	0.01
$U_g = 8.0$ m/s, $G_s = 200$ kg/(m^2 s)	0.11
$U_g = 8.0$ m/s, $G_s = 400$ kg/(m^2 s)	0.21

radial solids concentration (Fig. 5), one can conclude that the appearance of core–annulus flow structure with a dilute uniform core region surrounded by a dense annulus region in the bottom region coincides with high solids volumetric concentrations of more than 0.1, which also corresponds to the establishment of S-shaped axial solids distribution profile in the riser. Further increasing G_s and/or decreasing U_g only leads to a significant increase in solids concentration in the region $r/R > 0.6$, and this quick increasing density region extends inwards with increasing cross-sectional average solids concentrations. This indicates that the operating conditions have greater influence on the wall region than on the core region. This core–annulus flow structure in the dense bottom region, which has also been observed by other researchers (e.g. [45,46]), is clearly different from that in a bubbling fluidized bed, where a rather uniform radial solids distribution profile has been found [47].

3.3. Radial particle velocity profiles in the bottom region

Up to now, only limited experimental local particle velocity data are available in the literature for the riser bottom region with FCC particles. The time average upflowing and downflowing particle velocities, $V_{p,up}$ and $V_{p,down}$, respectively, are plotted in Fig. 6 as a function of the radial distance from the column axis for $Z = 1.5$ m and at a fixed $G_s = 50$ kg/(m^2 s) and $U_g = 2$, 3.5 m/s and for the same location with $U_g = 8$ m/s and $G_s = 200$ and 400 kg/(m^2 s).

It can be seen clearly in Fig. 6 that the particles move both up and down across the whole section in the bottom region, but the shapes of the radial profiles are different for the upflowing and downflowing particle velocity. For the upflowing velocity, $V_{p,up}$, the maximum always appears at the central region and $V_{p,up}$ has a relatively flat radial distribution at the center region, but a very steep velocity decrease as the radial position shifts towards the wall. The flatter particle velocity zone and the steep zone correspond to the dilute uniform core region and the dense wall region, respectively. At $U_g = 8$ m/s, the maximum and minimum $V_{p,up}$ (at $r/R = 0.0$ and 0.98, respectively) vary slightly with G_s. The area of the high and uniform $V_{p,up}$ region in the core region extends outwards towards the wall as the cross-sectional average solids concentration decreases, e.g. with increasing U_g at a given G_s or decreasing G_s at a constant U_g. Furthermore, it can be observed that $V_{p,up}$ does not change significantly at the wall for all operating conditions remaining approximately equal to 0.8 m/s, which may be attributed to the strong wall effects and dense conditions. Under all operating conditions, the largest $V_{p,up}$ appears at the center, and decreases with increasing r/R and reaches its lowest magnitude at the wall. Comparing with $V_{p,up}$, $V_{p,down}$ changes insignificantly with radial positions in the bottom region. The only exception happens for the operating condition of $U_g = 3.5$ m/s and $G_s = 50$ kg/(m^2 s), where the largest magnitude of $V_{p,down}$ appears in the middle region of $r/R = 0.7$–0.8. Increasing G_s at a given U_g appear to have no effects either on the value or on the radial profile of $V_{p,down}$. It reflects that in the dense bottom region the downflowing particle movements are dominated by particle–particle interactions, and

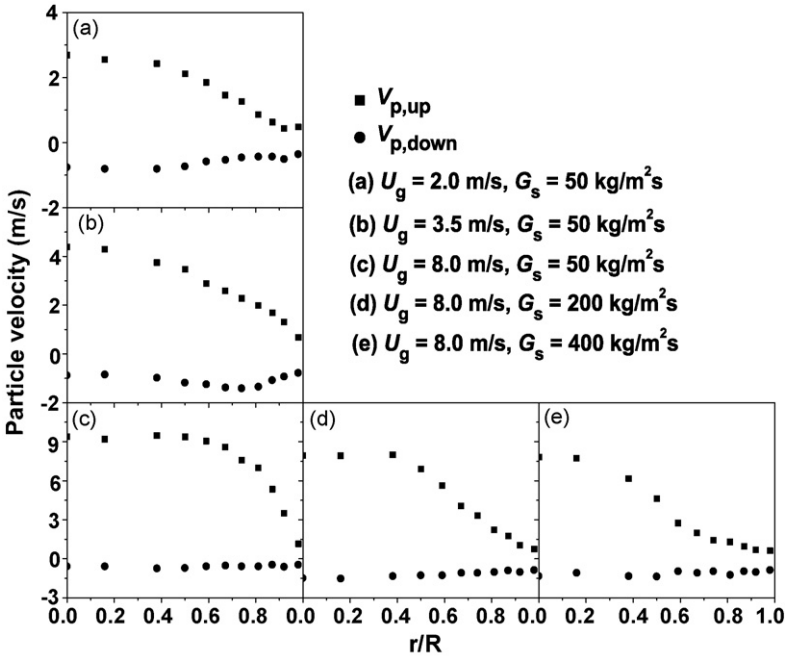

Fig. 6. Particle velocity profiles in 0.076 m riser under various operation conditions.

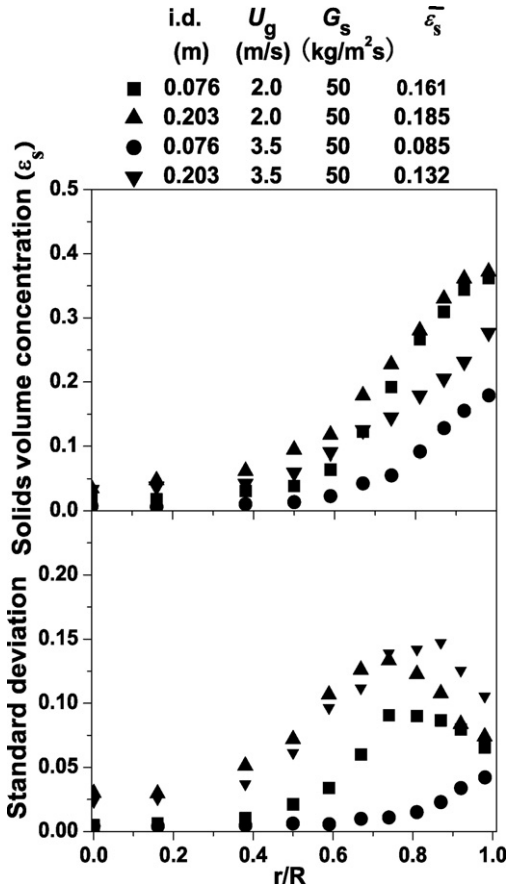

Fig. 7. Effects of column diameter on the radial solids concentration and fluctuation distribution in riser bottom region.

the downward movements of particles are further impeded by high-density conditions towards the wall.

3.4. Effects of column diameter on the radial solids concentration profile

Fig. 7 shows the radial solids distribution profiles in the bottom regions ($Z = 1.5$ m) of 76- and 203-mm diameter risers for a fixed solids flux of 50 kg/(m^2 s) and superficial gas velocities of 2 and 3.5 m/s. The results clearly show a relationship between column diameter and the cross-sectional average solids concentration. Under the same operating conditions, the larger riser is much denser than the smaller one, especially at $U_g = 3.5$ m/s, with $\bar{\varepsilon}_s = 0.085$ in the 76-mm diameter riser and $\bar{\varepsilon}_s = 0.132$ in the 203-mm diameter riser. The most significant differences are in the near wall region ($r/R > 0.5$). More explanation has been provided elsewhere [40]. However, there are no significant changes in the general trend of the profiles, all of which have a dilute and uniform central region and a dense annulus region where the solids holdup increases sharply toward the wall.

The corresponding radial profiles of the standard deviation of solids concentration fluctuations in Fig. 7 also confirm the marked influence of the column size. The larger diameter riser results in a higher solids concentration, and consequently increases the tendency of solids aggregation and the magnitude of fluctuations, reflected by the higher standard deviations. The

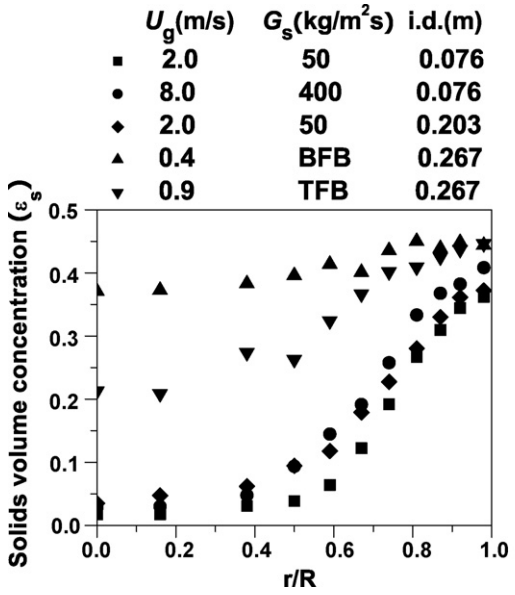

Fig. 8. Comparison of radial solids concentration distribution in the riser bottom region and TFB/BFB.

higher standard deviation in fluidized bed suggests a more vigorous particle–particle interactions and gas–particle interactions at that position [11,21]. The maximum standard deviation always occurs at some distance from the wall, except for the lean case ($\bar{\varepsilon}_s < 0.1$), where the maximum location is at the wall. And, the location of the maximum standard deviation moves slightly inwards with increasing average cross-sectional averaged solids concentration. Issangya et al. [21] also reported a similar trend of the maximum standard deviation locations, and they further treated this phenomenon as a possible distinguishing feature of high-density risers.

3.5. Bubbling or turbulent flow regime?

Although in the literature there are few papers focused on the bottom dense region in a CFB riser, significant controversy

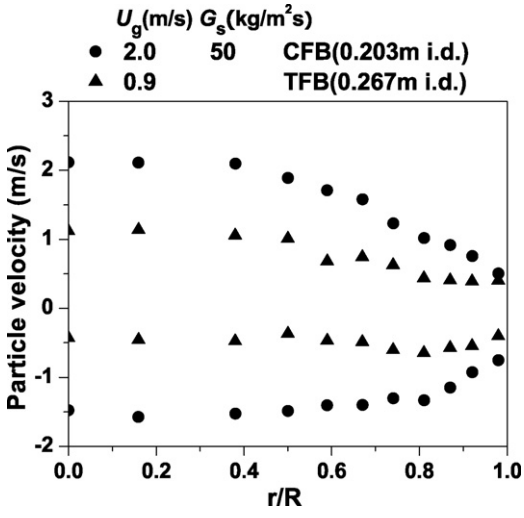

Fig. 9. Comparison of radial particle velocity profiles in TFB and CFB.

still remains about this section, especially about the kind of flow regime in this region. In order to give a clear comparison between the flow characteristics in the bottom dense region of the riser, the bubbling bed and the turbulent fluidized bed regime, the local flow properties, including solids concentration, particle velocity, and probability distribution, are examined in detail for the three regimes. To facilitate direct comparison, measurements of solids concentration were taken in a bubbling and a turbulent fluidized bed with the same optical fiber probe as used in the risers. The superficial velocity in the conventional fluidized bed (0.276 m in diameter, settled bed height 1.2 m) were at 0.4 and 0.9 m/s, corresponding to bubbling and turbulent flow regime (BFB and TFB, respectively). Measurements were taken at the height of 1.1 m. Static bed height was kept at 1.4 m. For comparison, the operating conditions in the 76- and 203-mm risers were $U_g = 2.0$ m/s with $G_s = 50$ kg/(m^2 s) and $U_g = 8.0$ m/s with $G_s = 400$ kg/(m^2 s), and the measuring level was $Z = 1.5$ m. High-density conditions were established in both cases with the cross-sectional average solids concentration of 0.16–0.21.

Fig. 8 compares the local solids concentrations for the three fluidized beds. All the solids concentration profiles show a trend of increased solids concentration with increasing radial distance. However, the variation is much greater in the risers increasing from about 0.05 to 0.35, whereas the change for the BFB case is just from 0.37 to 0.44 and for the TFB was from about 0.2 to 0.44. The most obvious differences occur in the central region. Towards the wall, the differences become smaller. From the above analysis, the flow structure in the bottom denser region of risers are apparently different than that in the bubbling fluidized bed. However, just based on the radial profiles of solids concentration, it is difficult to judge whether the riser bottom behaves as a turbulent fluidized bed.

Fig. 9 compares radial time mean particle velocity profiles in a turbulent fluidized bed and in a riser of nearly similar size. It can

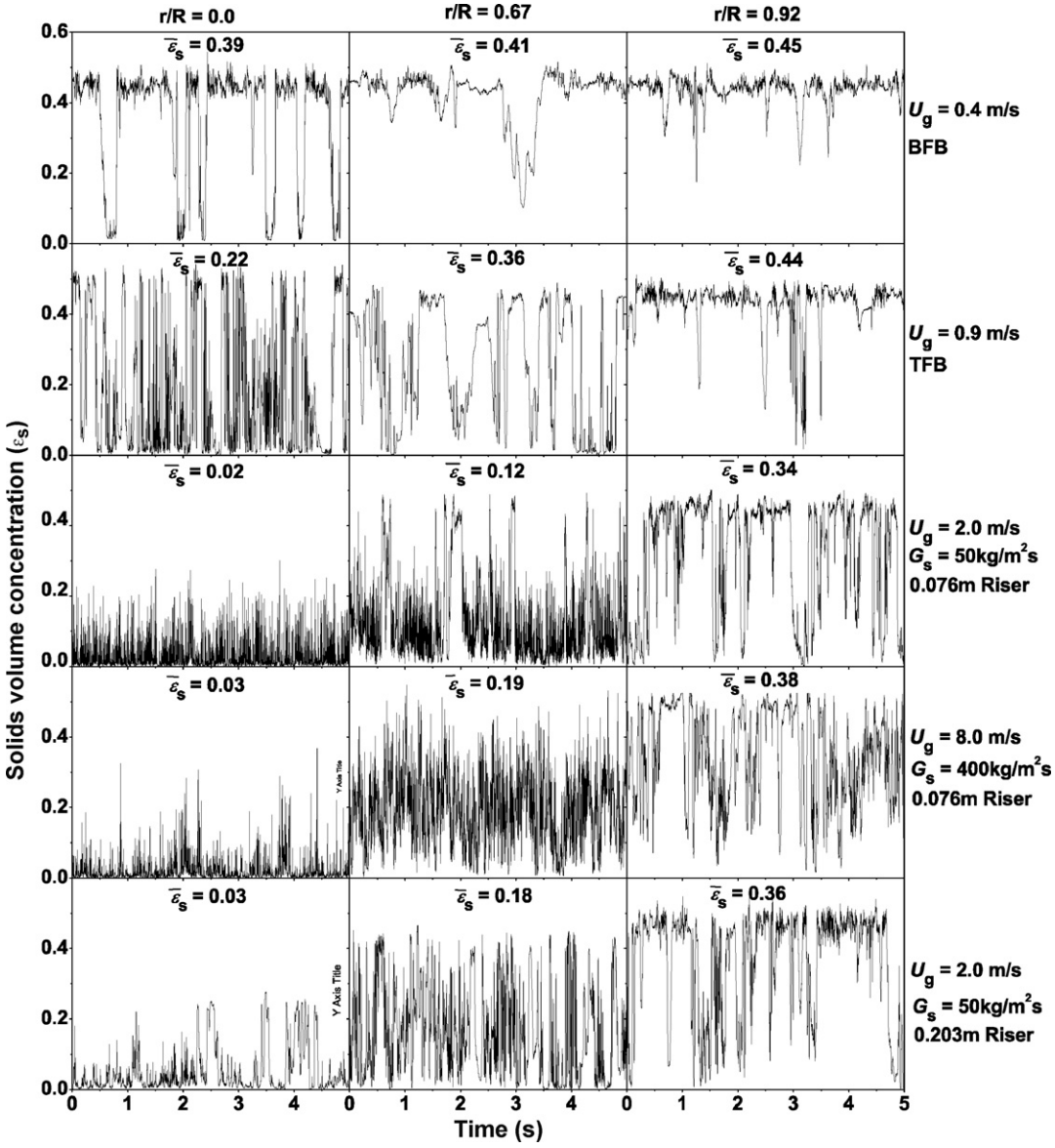

Fig. 10. Comparison of typical solids concentration fluctuation signals for four fluidization conditions at three radial positions.

be seen that both upflowing and downflowing particle velocities ($V_{p,up}$ and $V_{p,down}$, respectively) are significantly lower in the turbulent fluidized bed, especially in the central region. In addition, the measured frequencies of $V_{p,up}$ and $V_{p,down}$ are different in the two fluidized beds. In the core region, the time fraction of upflowing particle velocity were 61% in the turbulent fluidized bed and 86% in the riser bottom region, while in the near wall region, this ratio decreased to 45 and 55% for the TFB and riser, respectively. As a result, there are some difference between the much more fractions of particle upflowing upwards in both the center and the wall regions of CFB, indicating much less solids backmixing. Therefore, there are differences between the particle movements in the riser bottom region and the turbulent fluidized bed, especially in the core region.

Time-series solid concentration signals at three radial positions ($r/R = 0.0$, 0.67 and 0.92) are presented in Fig. 10 to compare the dynamic gas–solids flow behaviors in these different fluidized beds. For reference purposes the corresponding time-averaged solids concentration are also included. As shown in Fig. 10, the solids concentration signal fluctuates between zero, when the probe tip is within the bubble/void phase, and a high value (~0.52), corresponding to the dense/cluster phase. Significant differences among the signals can be seen for these different fluidized beds.

Fig. 10 shows that, in the bubbling regime ($U_g = 0.4$ m/s), the signals mainly reside at a base level of about 0.45 with frequent interruptions from bubbles, represented by the sharp decrease of solids concentration to near zero. A relatively stable dense

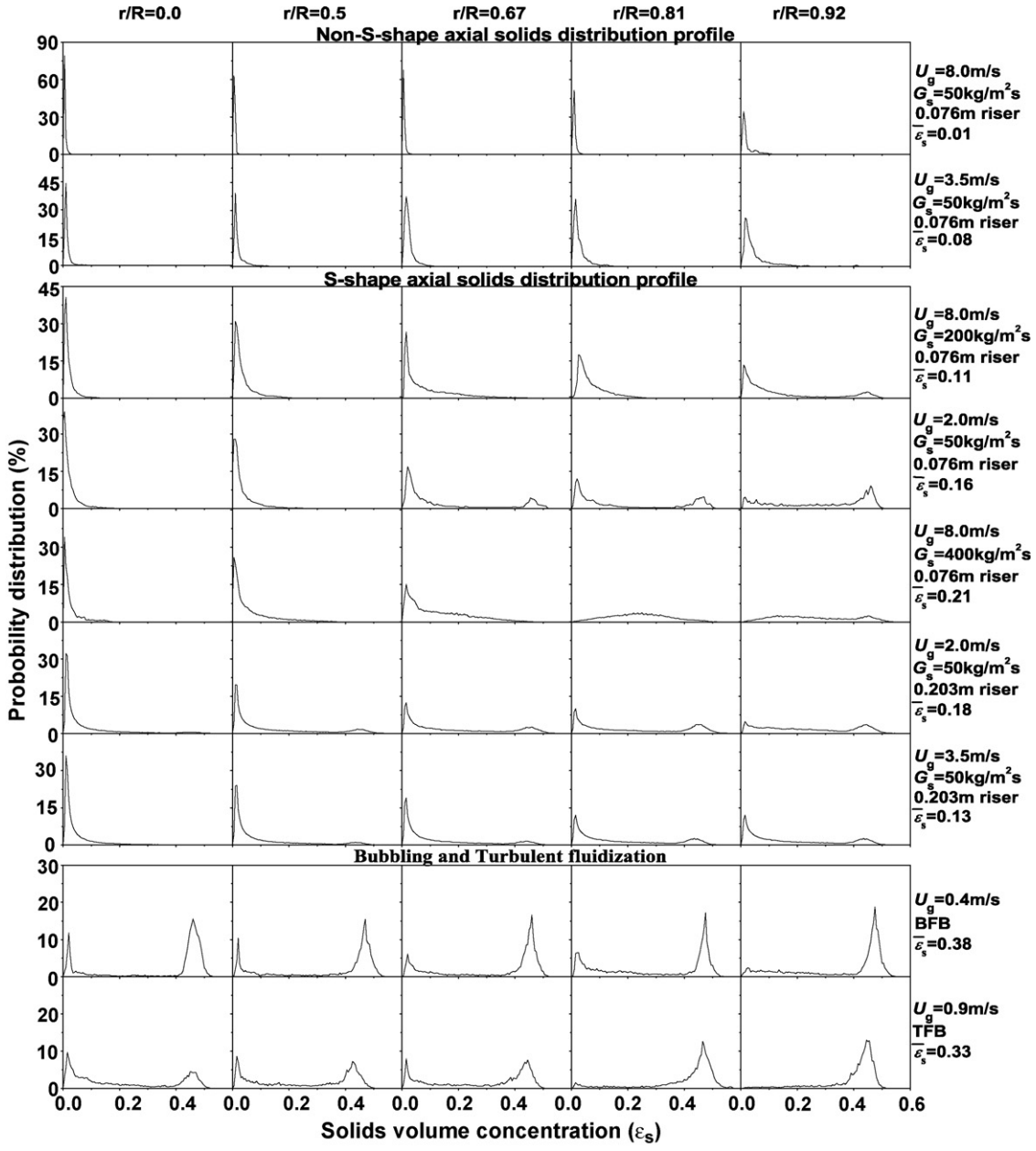

Fig. 11. Comparison between the probability density distribution of local solids concentration in bottom region of CFB and TFB.

phase exists at all three radial positions, indicating the solids phase is the continuous phase in the bubbling fluidized bed with dispersed bubble phase. When the bed is operated in the turbulent fluidization regime ($U_g = 0.9$ m/s), there is quite a difference between the signals in the center region and the near wall region. The signals in the wall region still remains at a high level with some sharp decreases, but in the central region the stable dense phase is no longer observed, reflecting the breakdown of regular bubble–dense phase flow structure. This change can be related to the formation of core–annulus flow structure in the turbulent fluidization regime, as shown in Fig. 8.

In the bottom dense region of the risers, the solids concentration in the central region mainly stays at low values with an absence of plateaus of high concentration. The peaks in the solids concentration signal represent passage of solids aggregates [19,48]. As for the near wall region, the signals shift to higher solids concentration, with a time-averaged value of 0.34–0.38. These results are consistent with that reported by Lin et al. [38], but they only compared the transient measurements in the central region of fluidized bed. From the above analysis, it can be noted that there is a great similarity in the nature of instantaneous flow structure in the bottom dense region of risers and that in the center and middle region of the turbulent fluidized bed. Furthermore, at all radial positions the solids volume concentration signals measured in the risers are obvious different from those of the bubbling bed. It is reflected by the facts that the stable plateaus of high solids concentration are rarely observed and the intensity of fluctuations is significantly higher than that in bubbling flow regime. Even in the near wall region, the instantaneous solids concentrations are always higher than 0.05, totally solid-free bubbles are rarely seen. In the contrast, in the bubbling fluidized bed, the bulk of bubbles contain few solids, indicated by the appearances of steep decrease to near zero.

To further characterize the phase structures and the interaction between the gas and solid phases in the different fluidization conditions, the probability density distribution (PDD) analysis of the solids concentration signals are carried out. Examining the shape of PDDs and comparing their peaks and tails can be used to reveal the changes in the dynamic gas–solids distribution [49,50]. The probability density distributions at different operating conditions and different fluidization systems are presented in Fig. 11. Depending on the operating conditions and the spacial locations, single- or two-peak PDD profiles are observed. The peak in the low/high solids concentration section represents the solids concentrations in the dilute/dense phase [50]. Two-peak plots represent the coexistence of dilute and dense phase, and the single-peak plots indicate the flow is dominated by just one phase. A flatter and wider distributed PDD likely indicates a better-mixed flow state and more intensive gas–solids interaction. Generally, decreasing gas velocity or increasing solids flow rate leads to an decrease of the peak in dilute phase and increase of the peak in dense phase, as well as a longer tail on the right hand side of the dilute phase peak and on the left hand side of the dense phase peak.

When comparing the shapes of PDDs with the corresponding cross-sectional average solids concentration ($\bar{\varepsilon}_s$), it can be found that in the bottom region of the risers, when $\bar{\varepsilon}_s \leq 0.1$, the PDD curves exhibit a single sharp peak at all radial positions, with peaks at solids concentration of less than 0.02. This narrow range of solids concentration distribution represents a homogenous dilute gas–solid suspension, which belongs to a dilute transport regime. However, when $\bar{\varepsilon}_s$ is increased beyond 0.1, two different types of PDDs are observed. For the region of $r/R < 0.5$, the PDD curves still keep the single-peak distribution, like that in dilute transport. When moving outwards towards the wall, the PDD shifts to two peaks with a continuous solids concentration. It is clear that the PDD profiles in the bottom of the risers are different than that in the bubbling fluidized bed where a clear two-peak PDD is observed with larger dense phase peak and almost no singles for the solids concentration between 0.1 and 0.4, indicating a pure two-phase flow structure. Obviously, the bubbling flow regime is not established in the bottom region of the riser. As illustrated in Fig. 11, however, there are more similarities between the PDDs in the region of $r/R > 0.5$ in the bottom dense region of the risers ($\bar{\varepsilon}_s > 0.1$) and the region of $r/R < 0.67$ in TFB: flat and continuous PDD over a wide range of solids concentration and two-peak PDD with larger peak in dilute phase.

These findings lead to the conclusion that it is not suitable to simply sort the whole bottom dense region in the riser as a currently existing flow regime, such as bubbling or turbulent flow regime. Depending on the values of the cross-sectional solids concentrations, there are two different flow patterns in the bottom region of the riser. For $\bar{\varepsilon}_s \leq 0.1$, corresponding to the non-S-shaped axial solids distribution, the flow structures in the bottom region may be treated as dilute transport flow. When $\bar{\varepsilon}_s > 0.1$ where a S-shaped axial solids distribution appears, the characterization of fluidization shows a gradual transition from the dilute transport flow regime to the turbulent flow regime when moving from the central region to the wall. Fig. 11 further demonstrates that the gas–solids phase structure may be different even when there is no or little difference in the time-average local solids concentration, as shown by the marked difference among PDDs in the wall regions of risers, and the bubbling and turbulent fluidized bed.

4. Conclusions

The study reported in this paper seeks to improve the understanding of the complex hydrodynamic behavior in the bottom region of CFB risers. Experiments were carried out in the bottom region of two risers with FCC particles over a wide range of operating conditions. The results include radial solids concentration and corresponding radial profiles of standard deviation, particle velocity profiles, and probability density distributions. Comparisons are made between the flow structures in the riser bottom region and that in bubbling and turbulent fluidized bed.

According to the cross-sectional average solids concentration ($\bar{\varepsilon}_s$), two kinds of the riser bottom regions are identified: dilute bottom region with $\bar{\varepsilon}_s < 0.1$ (non-S-shaped axial solids concentration profile) and dense bottom region with $\bar{\varepsilon}_s > 0.1$ (S-shaped axial solids concentration profile). For the dilute bottom region, the flow structure belongs to homogenous dilute phase flow. For

the dense bottom region, a core–annulus flow structure with a uniform dilute core region surrounded by a dense-annular zone appears. The characterization of fluidization shows a gradual transition from homogenous dilute phase flow to turbulent flow regime when moving from the center to the wall.

The influences of operating conditions mainly occur in the central region $r/R > 0.5$. At the same operation conditions, the larger riser appears somewhat denser than the smaller one. Particle velocity measurements show that the values of average solids upflowing velocity are significantly increased by increasing U_g and/or decreasing G_s, especially in the central region. However, the average downflowing particle velocity changes little with radial positions, suggesting that in the bottom region, the downward movement of particles is dominated by particle–particle interactions. For the high-density and high solids flux conditions, both the upflowing and downflowing particle velocities decrease with increasing solids flux.

References

[1] K.S. Lim, J.X. Zhu, J.R. Grace, Hydrodynamics of gas–solid fluidization, Int. J. Multiphase Flow 21 (1995) 141–193.

[2] R. Dry, C.J. Beeby, Applications of CFB technology to gas–solid reactions, in: J.R. Grace, A.A. Avidan, T.M. Knowlton (Eds.), Circulating Fluidized Beds, Black Academic & Professional, London, 1997, pp. 441–465.

[3] J.R. Grace, H.T. Bi, Introduction to circulating fluidized beds, in: J.R. Grace, A.A. Avidan, T.M. Knowlton (Eds.), Circulating Fluidized Beds, Chapman & Hall, London, 1997 (Chap.1).

[4] Y. Li, M. Kwauk, The dynamics of fast fluidization, in: J.R. Grace, J.M. Matsen (Eds.), Fluidization, Plenum Press, New York, 1980, pp. 537–544.

[5] M.J. Rhodes, M. Sollaart, X.S. Wang, Flow structure in a fast fluid bed, Powder Technol. 99 (1998) 194–200.

[6] U. Lackermeier, C. Rudnick, J. Werther, A. Bredebusch, H. Burkhardt, Visualization of flow structures inside a circulating fluidized bed by means of laser sheet and image processing, Powder Technol. 114 (2001) 71–83.

[7] N. Yang, W. Wang, W. Ge, J.H. Li, CFD simulation of concurrent-up gas–solid flow in circulating fluidized beds with structure-dependent drag coefficient, Chem. Eng. J. 96 (2003) 71–80.

[8] J. Adánez, P. Gayán, F. García-Labiano, L.F. de Diego, Axial voidage profiles in fast fluidized beds, Powder Technol. 81 (1994) 259–268.

[9] M. Horio, H. Ishii, M. Nishimuro, On the nature of turbulent and fast fluidized beds, Powder Technol. 70 (1992) 229–236.

[10] D. Bai, E. Shibuya, Y. Masuda, N. Nakagawa, K. Kato, Flow structure in a fast fluidized bed, Chem. Eng. Sci. 51 (1995) 957–966.

[11] A.S. Issangya, D. Bai, H.T. Bi, K.S. Lim, J. Zhu, J.R. Grace, Suspension densities in a high-density circulating fluidized bed riser, Chem. Eng. Sci. 54 (1999) 5451–5460.

[12] D. Bai, A.S. Issangya, J.R. Grace, Characteristics of gas-fluidized beds in different flow regimes, Ind. Eng. Chem. Res. 38 (1999) 803–811.

[13] A. Svensson, F. Johnsson, B. Leckner, Fluidization regimes in non-slugging fluidized beds: the influence of pressure drop across the air distributor, Powder Technol. 86 (1996) 299–312.

[14] Y. Cheng, F. Wei, G.Q. Yang, Y. Jin, Inlet and outlet effects on flow patterns in gas–solid risers, Powder Technol. 98 (1998) 151–156.

[15] S.W. Kim, G. Kirbas, H.T. Bi, C.J. Lim, J.R. Grace, Flow behavior and regime transition in a high-density circulating fluidized bed riser, Chem. Eng. Sci. 59 (2004) 3955–3963.

[16] B. Herb, S. Dou, K. Tuzla, J.C. Chen, Solid mass fluxes in circulating fluidized beds, Powder Technol. 70 (1992) 197–205.

[17] G.W. Xu, K. Nomura, N. Nakagawa, K. Kato, Hydrodynamic dependence on riser diameter for different particles in circulating fluidized beds, Powder Technol. 113 (2000) 80–87.

[18] J.H. Pärssinen, J.X. Zhu, Axial and radial solids distribution in a long and high-flux CFB riser, AIChE J. 47 (2001) 2197–2205.

[19] C.M.H. Brereton, J.R. Grace, Microstructural aspects of the behavior of circulating fluidized beds, Chem. Eng. Sci. 48 (1993) 2565–2572.

[20] M. Horio, H. Kuroki, Three-dimensional flow visualization of dilutely dispersed solids in bubbling and circulating fluidized beds, Chem. Eng. Sci. 49 (1994) 2413–2421.

[21] A.S. Issangya, J.R. Grace, D.R. Bai, J.X. Zhu, Further measurements of flow dynamics in a high-density circulating fluidized bed riser, Powder Technol. 111 (2000) 104–113.

[22] J.J. Nieuwland, R. Meijer, J.A.M. Kuipers, W.P.M. van Swaaij, Measurements of solids concentration and axial solids velocity in gas–solids two-phase flows, Powder Technol. 87 (1996) 127–139.

[23] A. Svensson, F. Johnsson, B. Leckner, Bottom bed regimes in a circulating fluidized bed boiler, Int. J. Multiphase Flow 22 (1996) 1187–1204.

[24] D. Bai, E. Shibuya, Y. Masuda, K. Nishio, N. Nakagawa, K. Kato, Distinction between upward and downward flows in circulating fluidized beds, Powder Technol. 84 (1995) 75–81.

[25] P. Schlichthaerle, J. Werther, Axial pressure profiles and solids concentration distributions in the CFB bottom zone, in: J. Werther (Ed.), Circulating Fluidized Bed Technology, vol. VI, German Society of Chemical Engineering, Frankfurt, 1999, pp. 185–190.

[26] J. Sternéus, F. Johnsson, B. Leckner, G.I. Palchonok, Gas and solids flow in circulating fluidized beds—discussion on turbulence, Chem. Eng. Sci. 54 (1999) 5377–5382.

[27] L.F. de Diego, P. Gayán, J. Adánez, Modelling of the flow structure in circulating fluidized beds, Powder Technol. 85 (1995) 19–27.

[28] M.R. Hyre, L.R. Glicksman, Axial and lateral solids distribution modeling in the upper region of circulating fluidized beds, Powder Technol. 110 (2000) 98–109.

[29] Y. Zheng, X.T. Wan, Z. Qian, F. Wei, Y. Jin, Numerical simulation of the gas-particle turbulent flow in riser reactor based on k–ε–k_p–ε_p–Θ two-fluid model, Chem. Eng. Sci. 56 (2001) 6813–6822.

[30] S. Benyahia, A.G. Ortiz, J.I.P. Paredes, Numerical analysis of a reacting gas/solid flow in the riser section of an industrial fluid catalytic cracking unit, Int. J. Chem. Reactor Eng. 1 (2003) (Article A41).

[31] A.K. Das, J. De Wilde, G.J. Heynderickx, G.B. Marin, J. Vierendeels, E. Dick, CFD simulation of dilute phase gas–solid riser reactors. Part I. A new solution method and flow model validation, Chem. Eng. Sci. 59 (2004) 167–186.

[32] H. Hatano, M. Ishida, The entrainment of solid particles from a gas–solid fluidized bed, J. Chem. Eng. Jpn. 14 (1981) 306–311.

[33] E.U. Hartge, D. Rensner, J. Werther, Solids concentration and velocity patterns in circulating fluidized beds, in: P. Basu, J.F. Large (Eds.), Circulating Fluidized Bed Technology, vol II, Pergamon Press, Oxford, 1988, pp. 165–180.

[34] M. Nakajima, M. Harada, M. Asai, R. Yamazaki, G. Jimbo, Bubble fraction and voidage in an emulsion phase in the transition to a turbulent fluidized bed, in: P. Basu, M. Horio, M. Hasatani (Eds.), Circulating Fluidized Bed, vol. III, Pergamon Press, Oxford, 1991, pp. 79–84.

[35] M. Louge, Experimental techniques, in: J.R. Grace, A.A. Avidan, T.M. Knowlton (Eds.), Circulating Fluidized Beds, Blackie Academic and Professional, London, 1997, pp. 313–368.

[36] H. Johnsson, F. Johnsson, Measurements of local solids volume-fraction in fluidized bed boilers, Powder Technol. 115 (2001) 13–26.

[37] H. Zhang, P.M. Johnston, J.X. Zhu, H.I. de Lasa, M.A. Bergougnou, A novel calibration procedure for a fiber optic solids concentration probe, Powder Technol. 100 (1998) 260–272.

[38] J. Werther, B. Hage, C. Rudnick, A comparison of laser Doppler and single-fiber reflection probes for the measurement of the velocity of solids in a gas–solid circulating fluidized bed, Chem. Eng. Process. 35 (1996) 381–391.

[39] Q. Lin, F. Wei, Y. Jin, Transient density signal analysis and two-phase micro-structure flow in gas–solids fluidization, Chem. Eng. Sci. 56 (2001) 2179–2189.

[40] A.J. Yan, J.X. Zhu, Scale-up effect of riser reactors (1): axial and radial solids concentration distribution and flow development, Ind. Eng. Chem. Res. 43 (2004) 5810–5819.

[41] M.L. Mastellone, U. Arena, The effect of particle size and density on solids distribution along the riser of a circulating fluidized bed, Chem. Eng. Sci. 54 (1999) 5383–5391.

[42] S. Malcus, G. Chaplin, T. Pugsley, The hydrodynamics of the high-density bottom zone in a CFB riser analyzed by means of electrical capacitance tomography (ECT), Chem. Eng. Sci. 55 (2000) 4129–4138.
[43] E.R. Monazama, L.J. Shadle, A transient method for characterizing flow regimes in a circulating fluid bed, Powder Technol. 139 (2004) 89–97.
[44] F. Wei, H.F. Lin, Y. Cheng, Z.W. Wang, Y. Jin, Profiles of particle velocity and solids fraction in a high-density riser, Powder Technol. 100 (1998) 183–189.
[45] G. Sun, Z. Chao, Y. Fan, M. Shi, Hydrodynamic behavior in the bottom region of a cold FCC riser, in: J. Werther (Ed.), Circulating Fluidized Bed Technology, vol. VI, German Society of Chemical Engineering, Frankfurt, 1999, pp. 179–184.
[46] S. Malcus, E. Cruz, C. Rowe, T.S. Pugsley, Radial solid mass flux profiles in a high-suspension density circulating fluidized bed, Powder Technol. 125 (2002) 5–9.
[47] R. Andreux, T. Gauthier, J. Chaouki, O. Simonin, New description of fluidization regimes, AIChE J. 51 (2005) 1125–1130.
[48] H. Ohara, H. Ji, A. Tsutsumi, K. Yoshida, Chaotic characteristics of local voidage fluctuation in a circulating fluidized bed, Can. J. Chem. Eng. 77 (1999) 247–252.
[49] R.F. Mudde, W.K. Harteveld, H.E.A. van den Akker, T.H.J.J. van den Hagen, H. van Dam, Gamma radiation densitometry for studying the dynamics of fluidized beds, Chem. Eng. Sci. 54 (1999) 2047–2054.
[50] H.P. Cui, N. Mostoufi, J. Chaouki, Characterization of dynamic gas–solid distribution in fluidized beds, Chem. Eng. J. 79 (2000) 133–143.